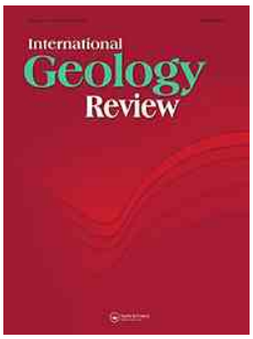

International Geology Review

ISSN: (Print) (Online) Journal homepage: https://www.tandfonline.com/loi/tigr20

Relict sand wedges suggest a high altitude and cold temperature during the Early Cretaceous in the Ordos Basin, North China

Yuchong Wang, Nan Peng, Hongwei Kuang, Fenghua Zhao, Yongqing Liu, Zhenrui Yang, Mingming Cui, Xiaoshuai Chen, Dawei Qiao & Kening Qi

To cite this article: Yuchong Wang, Nan Peng, Hongwei Kuang, Fenghua Zhao, Yongqing Liu, Zhenrui Yang, Mingming Cui, Xiaoshuai Chen, Dawei Qiao & Kening Qi (2023) Relict sand wedges suggest a high altitude and cold temperature during the Early Cretaceous in the Ordos Basin, North China, International Geology Review, 65:6, 900-919, DOI: 10.1080/00206814.2022.2081938

To link to this article: https://doi.org/10.1080/00206814.2022.2081938

Published online: 31 May 2022.

INTERNATIONAL GEOLOGY REVIEW
2023, VOL. 65, NO. 6, 900–919
https://doi.org/10.1080/00206814.2022.2081938

Taylor & Francis
Taylor & Francis Group

Relict sand wedges suggest a high altitude and cold temperature during the Early Cretaceous in the Ordos Basin, North China

Yuchong Wang [a,b*], Nan Peng [b*], Hongwei Kuang [b], Fenghua Zhao [a], Yongqing Liu [b], Zhenrui Yang [c], Mingming Cui [b], Xiaoshuai Chen [b], Dawei Qiao [b] and Kening Qi [b]

[a]College of Geosciences and Surveying Engineering, China University of Mining and Technology, Beijing, China; [b]Institute of Geology, Chinese Academy of Geological Sciences, Beijing, China; [c]Fangezhuang Mining Branch, Kailuan Clean Coal Co., Ltd, Tangshan, China

ABSTRACT

The Cretaceous, with relatively high atmospheric CO_2 concentrations, temperatures, and sea levels, is a typical greenhouse period in the geologic history of the Earth. Recently, gradual changes in the understanding of the Early Cretaceous climate have led to the proposal of small-scale polar glaciers or cooling events in polar regions. However, the cooling events in North China at mid-latitudes are still poorly understood. In this study, 48 wedge structures that are 35-240 cm wide and from 120 cm to more than 300 cm in depth down through the bottom of Lower Cretaceous Luohe Formation conglomerate and penetrated vertically downward into Jurassic Anding Formation mudstone in the Ordos Basin, North China. According to findings, these sand wedges are distinguished by large-scale V shapes, vertical to steeply dipping laminations and pebbles, aeolian abrasion of sand grains, ventifacts, upturned host strata, and other features that are most likely the source of thermal contraction cracking in periglacial desert region. The sand wedges formed when thermal contraction cracks were filled with wind-blown deposits and other material in dry, cold, and windy regions. This record may support the hypothesis that the Ordos Basin, western North China, may have been at a high altitude and was cold during the Early Cretaceous. During the Early Cretaceous, the complex topography and climate of North China allowed the Jehol Fauna to coexist with permafrost and glaciers.

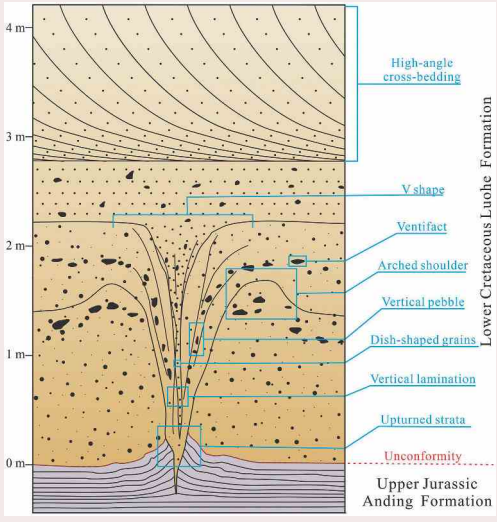

ARTICLE HISTORY
Received 24 February 2022
Accepted 22 May 2022

KEYWORDS
Early Cretaceous; cryogenic sand wedges; thermal contraction cracks; periglacial region; Ordos Basin; North China

1. Introduction

The Cretaceous period (145-66 Ma) is generally considered as a greenhouse period, with high global mean temperatures, weak latitudinal temperature gradients, relatively high and stable sea levels, and relatively high atmospheric CO_2 concentrations (Huber *et al*. 2002; Royer *et al*. 2007; Littler *et al*. 2011; Haq 2014; Wang

CONTACT Hongwei Kuang Kuanghw@126.com Institute of Geology, Chinese Academy of Geological Sciences, Beijing 100037,China; Fenghua Zhao zfh@cumtb.edu.cn College of Geosciences and Surveying Engineering, China University of Mining and Technology, Beijing 100083, China
*These authors contribution equally to this work.
This article has been corrected with minor changes. These changes do not impact the academic content of the article.

et al. 2014; O'Brien *et al*. 2017). In this warmer climate, various forms of life, namely the Early Cretaceous terrestrial Jehol Biota, are mainly distributed in North China and are at paleolatitudes of ~40°N latitude (Zhou 2014). However, in recent years, the records of Early Cretaceous abnormal climate fluctuation were found in North China at 30-40°N latitude: Cheng *et al*. (2002) believed that glacial debris flow deposits developed in the Lower Cretaceous at the northeastern margin of the Ordos Basin (Cheng *et al*. 2002); Wang *et al*. (1996) discovered red bed ice-rafted deposits in the Quantou Formation in the Songliao Basin (Wang *et al*. 1996); *Xenoxylon*, which represents a colder climate, is preserved in North China (Ding *et al*. 2016); Northeast China lacks thermophilic reptiles such as crocodiles (Zhou and Wang 2010); The pollen of cold and warm (conifers) plants coexist in North China (Zhong *et al*. 2019). The estimated average paleotemperature is approximately 10°C by Amiot *et al*. (2011), which is a present-day cool temperate climatic condition (e.g. modern Beijing, at 40°N latitude and 44 m altitude, has an average annual temperature of 10-13°C).

Gradual changes in the understanding of the Early Cretaceous climate have led to the proposal of small-scale polar glaciers or cooling events in polar regions (Alley and Frakes 2003; Rogov *et al*. 2017). The records of Early Cretaceous (Berriasian to Valanginian and Aptian) ephemeral high-latitude glaciations are sporadically reported, e.g. polished pavements, ice raft deposits, striated pebbles, glendonites, and periglacial structures (Alley and Frakes 2003; Frakes and Francis 1988; Frakes *et al*. 1995; Price 1999; Kuhnt *et al*. 2011). It is obviously difficult to systematically match with small-scale glaciers in polar regions and cold climatic conditions in mid-latitudes. The paleoclimate of North China where terrestrial organisms (such as the Yanliao Biota and Jehol Biota) flourish is much more complicated and has more controversy (e.g. Amiot *et al*. 2011; Liu *et al*. 2015; Ding *et al*. 2016; Zhou and Wang 2017; Zhang *et al*. 2021). Thus, some geoscientists have proposed the idea of high plateau in eastern China to explain the paradoxical phenomena occurring in North China (Li *et al*. 2008; Zhang *et al*. 2008, 2021; Xia *et al*. 2012). However, this view has not yet been confirmed by sedimentary and stratigraphic records.

Sand wedges are special sedimentary structures in extreme cold windy environments of periglacial regions (Murton 2013). They are unique arid landmarks and have important value in the palaeoclimatic reconstruction and research on polygon structures on other planets (Fábián et al. 2014; Li *et al*. 2014). Sand wedges are V-shaped cracks in the ground filled with primary debris, especially sand, that extend downwards into the ground to a maximum of several metres. The term 'sand wedge' is somewhat of a misnomer because the typical infill of these wedges ranges from silt to medium and coarse sand to pebbles (Black 1976; Williams 1986; Murton *et al*. 2000). Active sand wedges develop in present-day high-latitude or high-altitude cold and dry areas, such as the McMurdo Valley in Antarctica (Péwé 1959; Hallet *et al*. 2011; Mellon *et al*. 2014), the Nordic region (Watanabe *et al*. 2013; Andrieux *et al*. 2018), northern Canada (Fisher 1996; Bateman *et al*. 2015), and the Qinghai-Tibet Plateau (Jin *et al*. 2007). Previous studies indicate that permafrost is confined to regions that experience a mean annual air temperature no higher than –5°C, and periglacial structures commonly associated with permafrost are dependent on specific climatic conditions (Karte 1983; Williams 1986; Murton *et al*. 2000). Relict sand wedges in sedimentary rocks are main indicators of periglacial environments (Black 1976) and represent dry, cold, and windy periglacial climates with large temperature fluctuations in geological history.

In this paper, we describe relict sand wedges within medium- to coarse-grained clastic strata of the Lower Cretaceous Luohe Formation in the Hujiawan section, Ganquan, central Ordos Basin, western North China (Figure 1a), and we identify the existence of a periglacial zone from the perspective of sedimentological analysis and sedimentological origin. These structures are formed because of repeated thermal contraction cracks, reflecting discrete episodes of remarkably cold temperatures in the Ordos Basin during the Early Cretaceous. These new periglacial records, which is roughly contemporaneous with Jehol Biota, greatly extend the record of cold climates in mid-latitude regions. Regardless, the results contribute to a better understanding of diverse paleoclimates and paleo landforms of the Early Cretaceous in North China.

2. Geological background

North China, a term used to refer to the Chinese portion of the North China Craton, is one of the oldest blocks in the world, bounded to the west by the Helan Mountain, to the south by the Qinling Orogenic Belt and to the north by the Yinshan Orogenic Belt (Zhai 2011). The Ordos Basin, a large intracontinental composite basin with an area of approximately 320,000 km^2, is located in western North China (Figure 1). The Yinshan Orogenic Belt, Qinling Orogenic Belt, and Helan Mountain bounded it to the north, south, and west, respectively. The present eastern boundary of the Ordos Basin is the Luliang Mountain. However, during the pre-cretaceous period, the basin extended to the east of the Luliang Mountain (Liu *et al*. 2015; Zhao *et al*. 2020a). The Ordos Basin was developed based on Palaeozoic shallow marine deposits and Mesozoic terrestrial deposits (Zhang

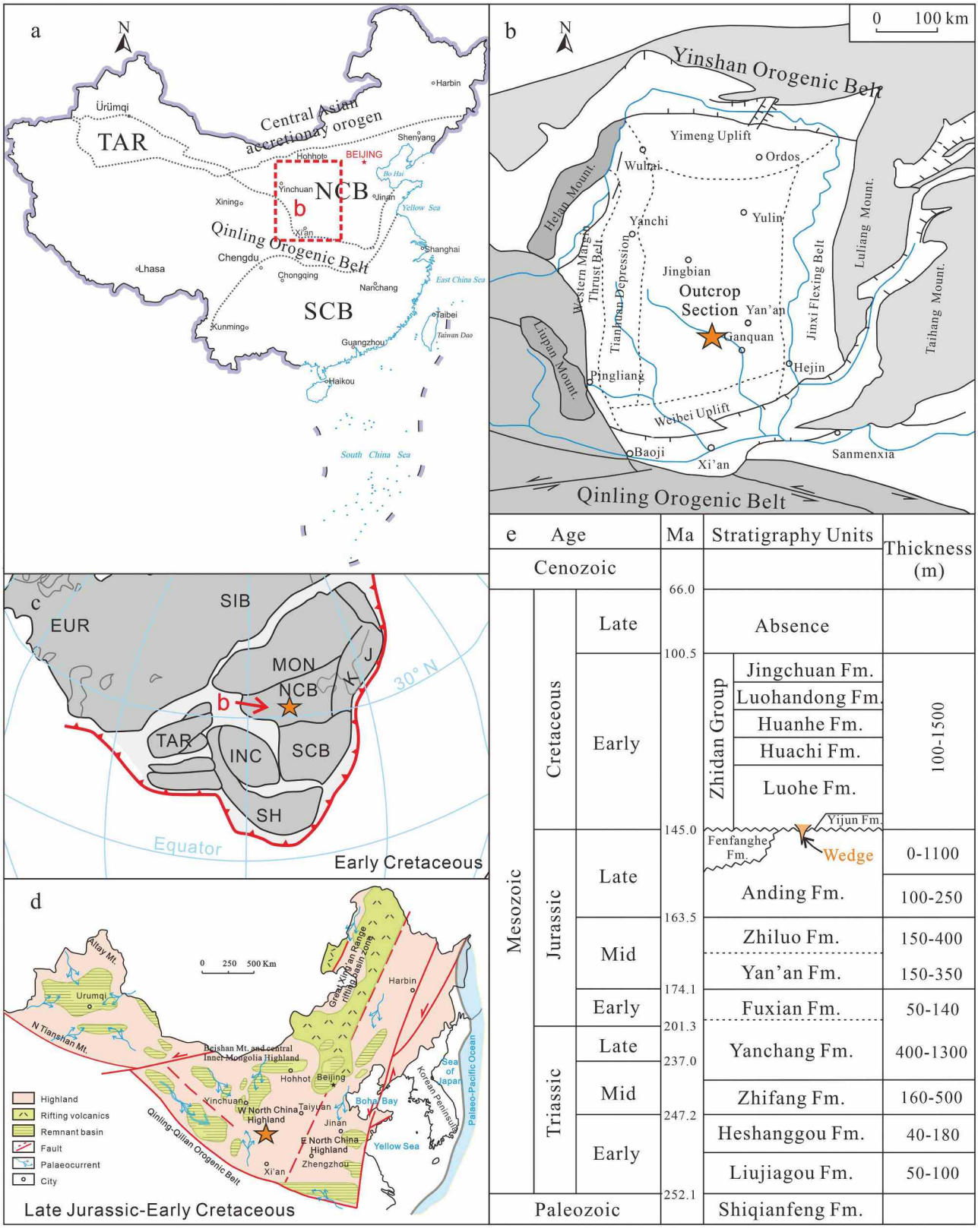

Figure 1. (a) Map of China and major cratonic blocks within China. (b) Simplified structural map of the Ordos Basin and location of outcrops (modified from Darby and Ritts 2002). (c) Palaeogeographic map of Eurasia during the early cretaceous. The yellow star is the site of the outcropping section. (Adapted from Enkin *et al*. 1992; Amiot *et al*. 2011; Meng *et al*. 2019). (d) The palaeogeographic map of North China from the Late Jurassic to the Early Cretaceous. (e) Stratigraphic column of the Ordos Basin (modified from Zhao *et al*. 2020ba). Fm., Formation; EUR, Europe; INC, Indo-China; IND, India; J, Japan; K, Korea; MON, Mongolian; NCB, North China; SCB, South China Basin; SH, Shan Thai; SIB, Siberian; and TAR, Tarim.

et al. 2019; Zhao *et al*. 2020b). Outcropping strata in the Ordos Basin, from east to west, are Cenozoic, Mesozoic, and Palaeozoic sedimentary strata. The Ordos Basin experienced multiphase evolutionary stages from Palaeozoic sedimentary marine facies and Mesozoic sedimentary continental facies to Cenozoic basin peripheral fault-depression activities, as confirmed by the sedimentary record and lithofacies (Zhang *et al*. 2019).

In the Ordos Basin, the Jurassic strata are divided into, from the bottom to top, the Fuxian Formation, the Yan'an Formation, the Zhiluo Formation and the Anding Formation (Figure 1e). The Anding Formation is composed of mostly mudstone, marlstone, sandstone, and interbedded marls, which are interpreted as lake and delta facies that were deposited under hot and arid conditions (Zhao *et al*. 2006). The Upper Jurassic Fenfanghe Formation is composed of unconformity-bound, coarse-grained clastic wedges of braided river facies confined along the southwestern and western Ordos Basin (Li *et al*. 2015). The stratigraphic sequence of the Lower Cretaceous in the Ordos Basin, from bottom to top, includes alluvial conglomerates of the Yijun Formation, aeolian sandstones of the Luohe Formation, saline lacustrine and lacustrine-fluvial rocks of the Huachi and Huanhe formations, aeolian and fluvial deposits of the Luohandong Formation, and mainly fluvial and lacustrine depositional systems of the Jingchuan Formation (Jiang *et al*. 2001; Qiao *et al*. 2020). The Yijun Formation occurs only on the southern margin of the Ordos Basin. In the Hujiawan section, the Luohe sandstone is deposited unconformably over the Anding Formation. Reported wedges are all present at the boundary between the Anding and Luohe formations in the Hujiawan section, Ganquan, central Ordos Basin, western North China (Figure 1).

To date, there is no direct dating record of the Luohe Formation. The magnetostratigraphic age of the Luohe Formation is ~141-135 Ma (Huang 2010). Based on records of *conchostracans* (Wang 1984; Li 2017), the lower part of the Zhidan Group, including the Yijun, Luohe and Huanhe formations, approximately corresponds to the Barremian stage of the Lower Cretaceous (Li 2017). Despite lacking volcanic ash, interbedded volcanic rocks, and fossils that could be used for radiometric dating, the age of the Luohe Formation has traditionally been considered as the Berriasian-Valanginian (Xi *et al*. 2019). Following the phase B of the Yanshanian orogenic event, conglomerates (e.g. Yijun Formation, Member II of Tuchengzi Formation) and aeolian sandstones (e.g. Luohe Formation, Santai Formation) were formed to affect the entire North China (Liu *et al*. 2015). As a result, the ages 143-135 Ma can be used as depositional ages for the Luohe Formation, and the active sand wedges in the Ordos Basin should be closed to 143 Ma. At the same time, the Barremian Yixian and Aptian Jiufotang formations yield a large amount of well-preserved fossils of various terrestrial organisms (Jehol Biota), e.g. eutherian and metatherian mammals, birds, many subgroups of insects, and angiosperms at the northern part of North China (Zhou 2014; Xu *et al*. 2020). In the paleotectonic reconstructions of the Early Cretaceous, North China, which is a part of Asia that was formed by the complicated collision of the North China, South China, Siberian, and Pacific plates (Meng *et al*. 2019; Zhao *et al*. 2020b), is placed between latitudes 30° and 40° north of the equator (Figure 1c) (e.g. Ma *et al*. 1993; Huang *et al*. 2008).

3. Methods

Through geological survey, more than 50 relict sand wedges were investigated and measured in the field, and two-dimensional wedge data, including the sand amount, spatial arrangement, individual morphology, size and orientation, were collected, and the filling was sampled. Based on microscopic observations under thin section microscopy (LEICA DM2500P microscope) and scanning electron microscopy (ZEISS EVO MA15 SEM), laboratory work primarily focused on the composition and structure of filling, such as the lithology, mineral compositions, and clasts counting. The SEM was executed in backscatter detector mode under a high vacuum with 5 kV and a working distance of 7.5 to 8.5 mm, where various magnifications (90× to 1200×) were used. The SEM samples came from vertically laminated sandstone near the centres of wedges. Samples comprise brownish-yellow sand with grains ranging in diameter from 0.05 to 1 mm. Grains 0.2 to 0.6 mm in diameter were examined with a SEM. SEM analysis was conducted at the Key Laboratory of Stratigraphy and Palaeontology, Institute of Geology, Chinese Academy of Geological Sciences (CAGS). Whole grains and magnified sections of typical features from quartz grains were photographed. The surface textures of grains from vertically laminated sandstone near the centres of wedges were compared with grains from the Lower Cretaceous Luohe Formation.

4. Results

4.1 Sedimentology of the Hujiawan section

The outcrop containing relict sand wedges is located at the boundary of the Anding and Luohe formations in Hujiawan village, 40 km NW of Ganquan City, Shaanxi

Province. Three units were delineated from bottom to top in the section, namely, unit 1, unit 2, and unit 3 (Figure 2).

4.1.1 Unit 1: laminated mudstone – shallow lacustrine deposits

Description. Unit 1 belongs to the uppermost part of the Upper Jurassic Anding Formation (Figure 2a and b) and is composed of more than 3 m-thick grey-purple laminated mudstone, marls, siltstone, and fine-grained sandstone (Figure 2c). The other parts of the Anding Formation appear to have been covered by roads and buildings. Trace fossils are present on the surface of fine-grained sandstone in other sections and grade into an alternation of medium thin-bedded fine-grained sandstone and mudstone (Figure 2c).

Interpretation. Laminated muds and marls are interpreted as shallow-water lacustrine deposits due to the settling of suspended sediments from water bodies (Kraus and Gwinn 1997; Scherer *et al*. 2007). Laminated fine-grained sandstone may be the product of the upper flow regime (Kraus and Gwinn 1997). During Middle Jurassic, the original sedimentary extent of the Ordos Basin was almost twice that of the present-day residual basin, and the subsidence centre of the Ordos Basin was close to the Hujiawan section at that time (Zhao *et al*. 2006, 2020b).

4.1.2 Unit 2: weakly layered pebbly sandstones – desert pavement deposits

Description. Unit 2 occurs in the bottom part of the Lower Cretaceous Luohe Formation (Figure 2a). It comprises 2-3 m-thick massive or weakly layered coarse- to fine-grained sandstones with interbedded conglomerates with clasts that are 1-10 cm in diameter, including clasts of quartz and opal (Figure 2d-g). Pebbles are subrounded and irregular in shape (Figure 2g). The surfaces of pebbles are smooth and coated with brown desert varnish, and some surfaces are pitted (Figure 2g). Although the largest pebbles are oriented chaotically in all directions, some of the long axes of clasts are parallel to bedding and positioned horizontally or in other orientations (Figure 2f).

Interpretation. The pebbles of unit 2 may be inherited from the braided pattern of ephemeral streams in arid environments (McFadden *et al*. 1987). The aeolian sand and pebble rhythms indicate sandsheet and aeolian pavement cycles, which may be related to variations in accommodation and sediment supply controlled by climate and tectonics. Pebbles reside at the surface and protect against wind erosion and fine-grained dust detachment (McFadden *et al*. 1987). The varnish on the surfaces of clasts, a black manganese-rich coating, is formed in arid environments by microbial mechanisms (Dorn and Oberlander 1981), but the formation mechanism remains unproven (Thiagarajan and Aeolus Lee 2004; Perry *et al*. 2006; Goldsmith *et al*. 2014). These massive or weakly layered sandstones and pebbles (Luohe Formation) formed in sandy-pebble deserts or desert pavement environments (Gobi in the Mongolian language) (Matmon *et al*. 2009; Shen *et al*. 2020).

4.1.3 Unit 3: large-scale cross-bedding sandstone – aeolian dune deposits

Description. Unit 3, which is tens of metres of massive and large-scale cross-bedding coarse sandstone (Figure 2d), also belongs to the lower part of the Lower Cretaceous Luohe Formation. Unit 3 comprises coarse- to medium-grained sandstone with uniform (well-sorted) grain sizes and subrounded to rounded grain surfaces. These sandstones are composed of quartz, feldspar, chert, and other minerals with well sorted and subangular to rounded in shape. These sandstones with large-scale high-angle planar cross-bedding and trough cross-bedding are arranged into cross-bedded sets reaching 2 to 10 m thick (Figures 2; Figure 3). The slope angle of cross-bedding is usually more than 25°, and the maximum is approximately 34°. Some cross-bedding sets are over 100 metres thick. Horizontal distribution generally exceeds 100 metres, with a maximum of several thousand metres. SEM microstructure analysis revealed dish-shaped and crescent-shaped impact scars that were unevenly distributed on the surface of quartz.

Interpretation. The well-sorted coarse sandstone of unit 3 (Luohe Formation) with large-scale cross-bedding is interpreted as an aeolian dune deposit (Hunter 1977; Clemmensen and Tirsgaard 1990; Xu *et al*. 2019). The Lower Cretaceous Luohe Formation is dominated by thick-bedded sandstones of aeolian desert facies (Jiang *et al*. 2001; Qiao *et al*. 2020). Qiao *et al*. (2022) reconstruct the prevailing surface-paleowind directions based on the dip-azimuths from large aeolian cross-bedding foresets, which indicate that the westerly wind prevailed in the Ordos Basin during the creation of the Luohe Formation. Mechanical surface textures, such as dish-shaped and crescent-shaped impact scars, result from direct impact by saltating and creeping grains under high-velocity wind transportation in an arid environment (Krinsley *et al*. 1976; Costa *et al*. 2013; Vos *et al*. 2014).

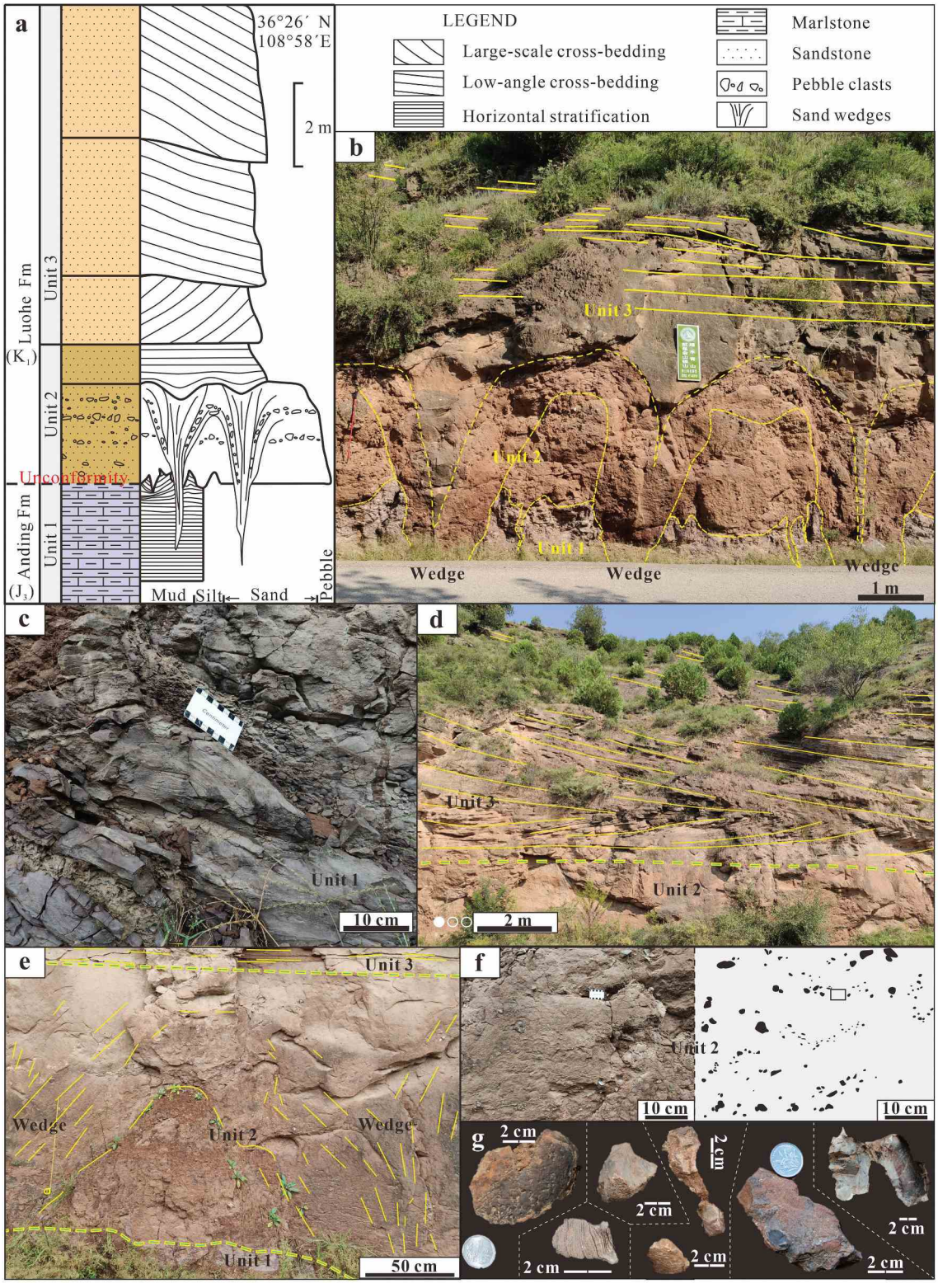

Figure 2. Characteristics of the Anding and Luohe formations in the Hujiawan section in the Ganquan, Ordos Basin. (a) Lithostratigraphy of the Hujiawan section in Ganquan in the Ordos Basin. (b) Grey mudstone and siltstone of unit 1. (c) Red thick-bedded sandstone with large-scale planar and trough cross bedding in unit 3. (d) Sandstone with sand wedges in unit 2. (e and f) Sandstone with interbedded conglomerate in unit 2. Some long axes are parallel to bedding in horizontal or other orientations. (g) Pebble-sized aeolian opal clasts in massive sandstone with subrounded and irregular shapes are ventifacts in unit 2. Unit 1 is the Anding Formation, and units 2 and 3 are the Luohe Formation. The dotted blue line is the boundary between the Anding and Luohe formations.

4.2 Description of wedges

4.2.1 Morphological characteristics

More than 48 relict sand wedges at the boundary between the Anding Formation and the overlying Luohe Formation occur in the section that is a total of 250 m long (Figure 2;Figure 3). Generally, the middle or upper parts of relict sand wedges show symmetrical wedges or V shapes with slightly curved boundaries (Figure 4). Relict sand wedges extend from unit 2 down into unit 1 and cut unit 1 (Figure 4a). They have maximum widths of 2.7 m and taper out downwards. Their vertical height reach 2.9 m. In most cases, the deeper the wedge is, the wider the wedge is. Some wedges display convex outwards or branching, saclike and occasionally intersecting morphologies (Figure 5f and g). Moreover, there are several thin sand veins that are 2-50 mm wide (Figure 5f and g) located between the relict sand wedges. As shown in Figure 4, they appear to be internally massive, and their sides range from sharp and planar

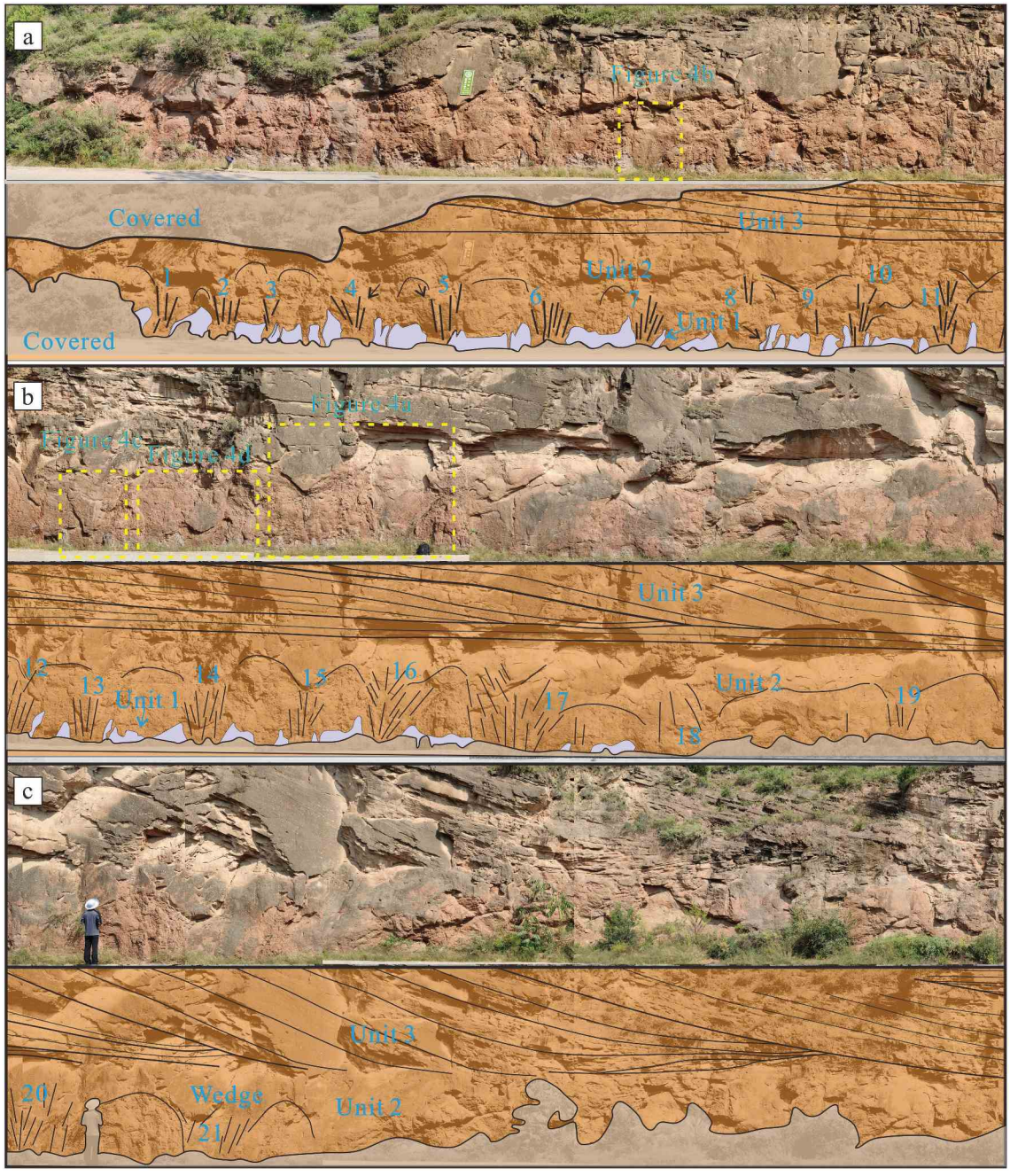

Figure 3. The outcrop containing relict sand wedges at the boundary of the Anding and Luohe formations in the Hujiawan section.

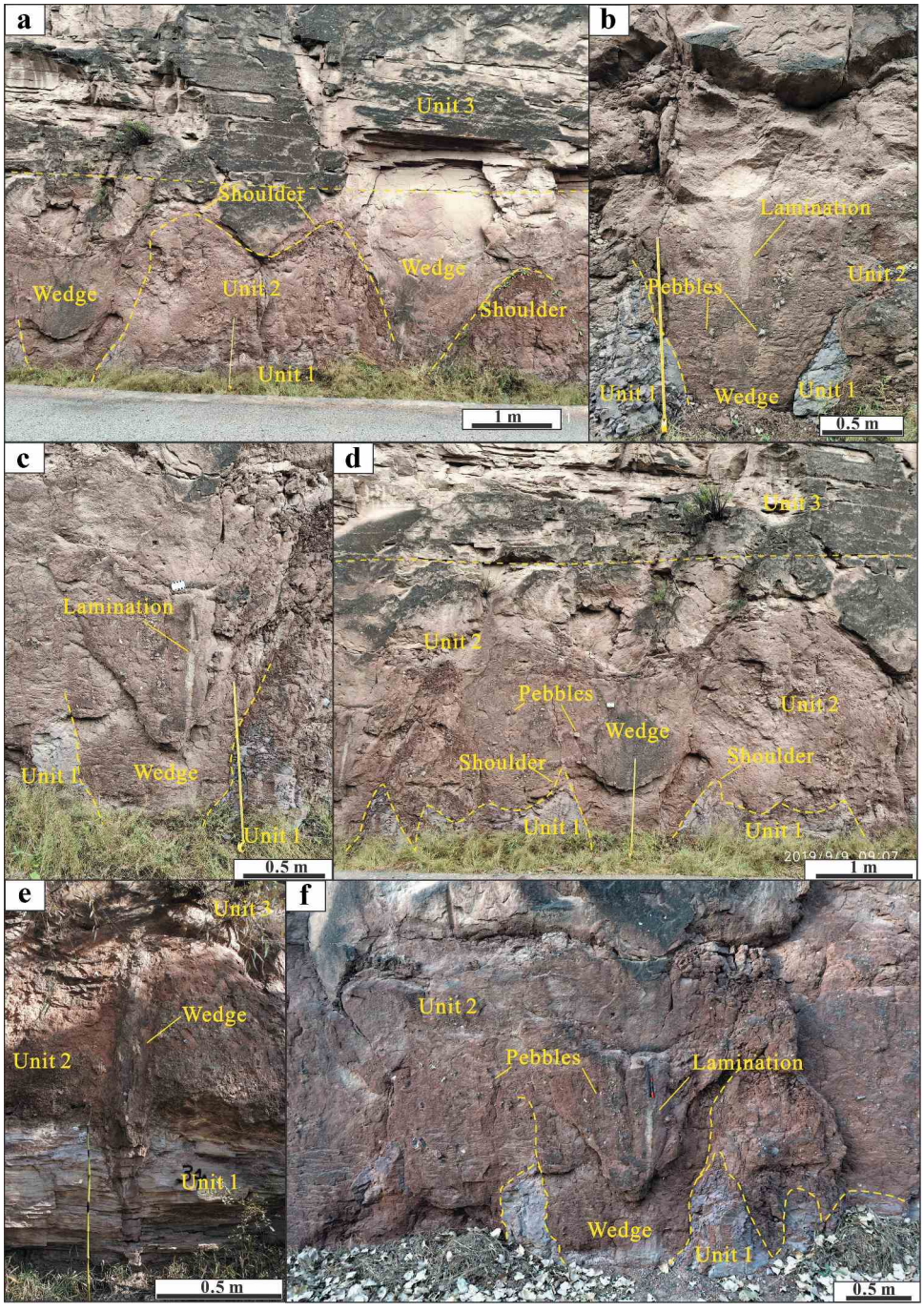

Figure 4. Macroscopic characteristics of sand wedges. (a) Outcrops showing the spatial arrangement of sand wedges in the Hujiawan section. (b) The macroscopic morphologies of relict sand wedges. Pebbles are concentrated upward and at or near the upper parts of relict sand wedges. (c and d) Pebbles are concentrated at vertical laminations in the sand wedges. (e) Adjacent rocks near the shoulder parts of the relict sand wedges are arched upwards.

to undulating. The wedges expand in many directions simultaneously with the morphology of the polygon in plan view. Unfortunately, the plan view of these polygons on the upper bedding surface is poorly detailed due to the lack of outcrops.

4.2.2 Filling characteristics

The fillings of wedges, which are significantly different from unit 1 but have the same colour, lithology, and texture as units 2 and 3, mainly comprise coarse- to fine-grained sands and low amounts of pebbles (Figure 4).

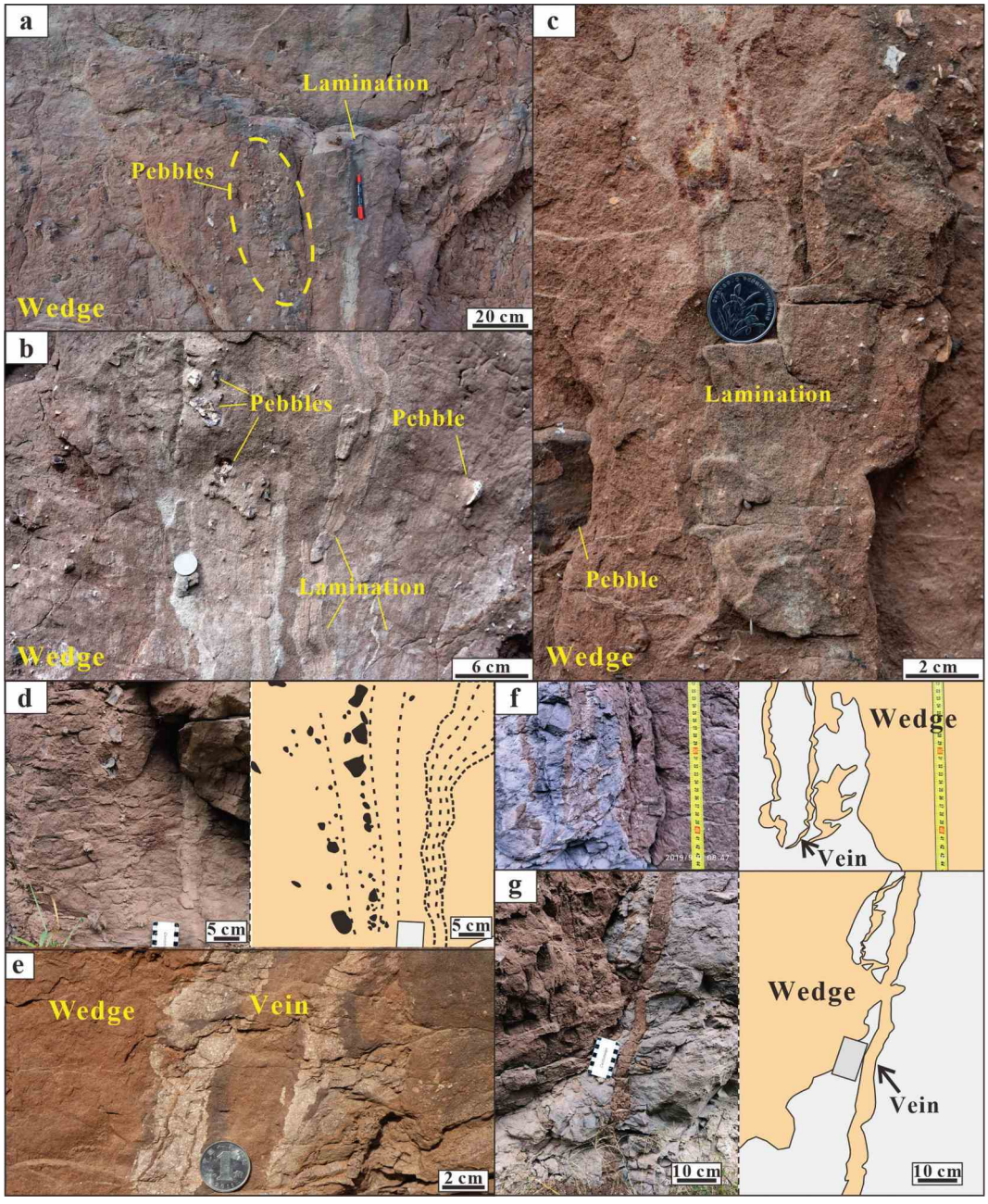

Figure 5. Characteristics of relict sand wedges in the Hujiawan section. (a-d) The longest axes of pebbles parallel to the wedge centres and edges. (e-g) Sand veins are 2-50 mm thick and 30–200 cm deep and occur singly.

The brown fillings are composed of quartz, feldspar, chert, dolomite, and other minerals and are well-sorted and subangular to rounded in shape (Figure 6). Fillings display coarsening-upwards, i.e. pebbles are concentrated upwards, but downwards, they exhibit intense heterogeneity and good textural maturity (Figure 5). Distinctly, both vertical laminations (on the scale of mm) of sands (Figure 6a and b) and the a-axis of pebbles inside wedges are parallel to the wedge boundary in some wedges (Figure 5). In some wedges, the particle size often distinctly decreases from one side to the other side (Figure 5a). The results of SEM analysis of quartz grains indicate that the microtextures, comprising well-rounded borders, smooth surfaces, and dish-shaped and crescent-shaped impact scars, are widespread (Figure 7). In particular, 3 kinds of surface textures, including dish-shaped (a-eFigure 7), bulbous edges (Figure 7b and f), and crescent-shaped impact scars (Figure 7c, g-h), are very conspicuous on the surfaces of quartz grains. Bulbous edges often coincide with

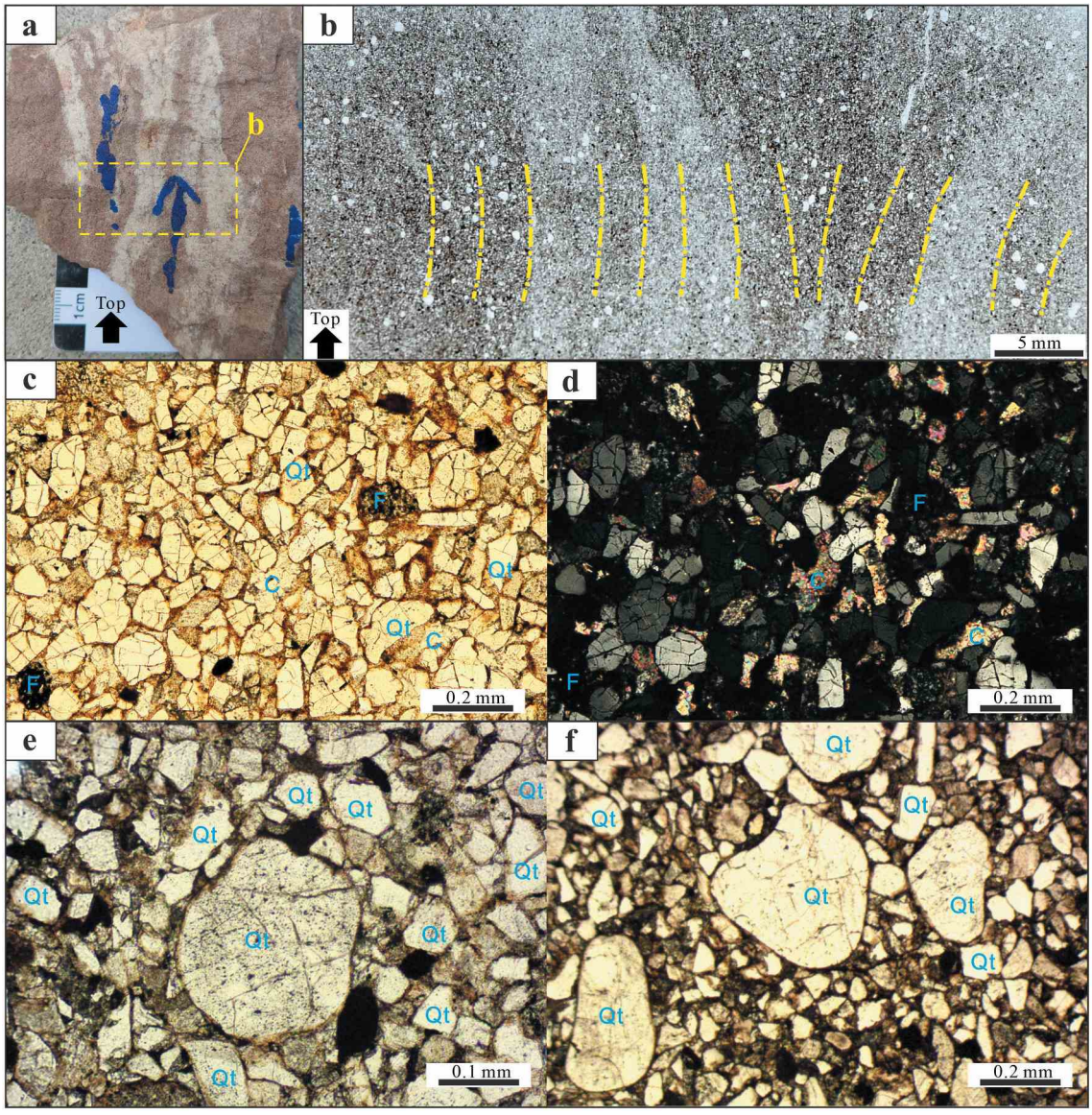

Figure 6. Microtextures of relict sand wedges in the Hujiawan section. (a and b) The diameter of grains decreases from one side to the other in the horizontal direction, which causes the wedge in the horizontal section to comprise multiple coarse-fine cycles. (c-f) The grains are quartz, feldspar, and carbonate, and are well- to poorly rounded, moderately well sorted grains. The monocrystalline quartz grains are dominant in all samples and are distinguished by the features of grain shattering. Note intra-granular microcracks in the quartz grains. Qt, quartz; F, feldspar; C, carbonate.

smoothed or polished elongated depressions (Figure 7e). Other microtextures of quartz might be camouflaged because of the matrix and diagenesis. Pebbles are chiefly quartz and opal, and dolomites are rare. The surfaces of pebbles are smooth and coated with desert varnish, the same as those in unit 2 (Figure 2g). Distinctly, both the laminations and a-axes of pebbles near the centres of relict sand wedges are generally vertical or nearly vertical, whereas those nearer the sides tend to be steeply dipping and parallel to the sides (Figure 5). The fillings display coarsening-upwards, and the amount of pebbles distinctly decreases with depth (Figure 4b). The fillings of the wedge are vertically laminated. The laminae are commonly 1-10 mm thick and a few tenths to a few metres high until converging at the bottom of the wedge (Figure 5; Figure 6a). These internal laminations and textures are also clear under the microscope (Figure 6b).

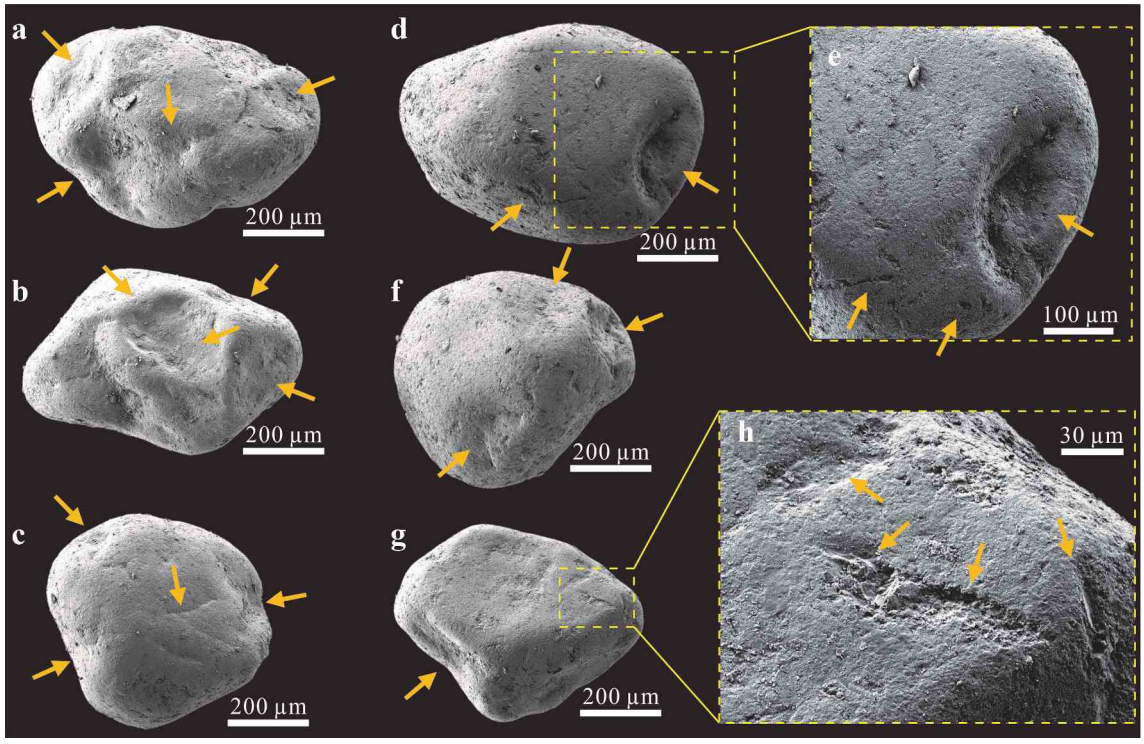

Figure 7. Scanning electron microscopy images of quartz-grain surface features from the middle parts of relict sand wedges. (a and b) Irregular pits of various sizes indenting a rounded quartz grain. (c-g) Smooth surfaces with bulbous edges and dish-shaped impact features. (h) Crescent-shaped impact scars on quartz surfaces. Image e is a scaled-up portion of image d. Image h is a scaled-up portion of image g.

5. Discussion

5.1 Periglacial sand wedges: the most possible explanatory cause

Wedge structures in sedimentary rocks can generally formed by desiccation (Kocurek and Hunter 1986; Loope and Haverland 1988; Velde 1999; Weinberger 2001), thermal contraction cracking (Murton *et al*. 2000), water escape (Murton *et al*. 2000; Moretti and Sabato 2007), earthquakes (Moretti and Sabato 2007; Burbidge *et al*. 2008), or a variety of triggers (Allen 1982; Black 1983; Murton *et al*. 2000) that resemble wedge structures in this study. Most of above-mentioned origins could easily be ruled out:

(i) Desiccation cracking: The sand veins and wedges that formed by desiccation cracking are small and closely spaced (Weinberger 2001); desiccation cracking can normally be excluded in gravel, sand, and other coarse materials (Velde 1999). In addition, all fillings of desiccation cracks have massive or parallel bedding, which are completely separate from the vertical bedding of the sand wedges (Murton *et al*. 2000).

(ii) Earthquake or rapid loading: Unlike sand wedges, wedge structures formed by earthquakes or rapid loading are a mixture of water-rich sand particles with a relatively uniform grain fabric structure (Owen and Moretti 2011). The diapirs or diapiric structures by earthquake or rapid loading showed significant soft deformation, which is obviously different from the sand wedge. In addition, diapiric structures must be accompanied by mutual penetration of sandy and muddy layers.

(iii) Deep ditch: Paleo-rills that form from deep ditches cut by running water or wind currents (Øygarden 2003) are often centimetres in length and depth. It is extremely difficult for water or wind currents to produce sand wedges with narrow, deep, sinuous and sharp wedge shapes (Murton *et al*. 2000).

(iv) Ice wedge: Massive filling of ice wedge casts occurs by thermo-karstification after ice melts (Péwé 1959). In contrast to the upturned strata adjacent to many primary sand wedges, ice wedge casts may be accompanied by down-turning and block faulting of host strata (Murton *et al*. 2000). Vertical lamination is the most crucial indicator of primary sand wedges because debris quickly fills the ice wedge once the ice melts.

Periglacial sand wedge controlled by thermal contraction cracking is the most likely explanation in this study, as discussed below.

5.1.1 The V-shaped formation is controlled by thermal contraction cracking

Cracks that begin at the surface and spread into the soils are known to occur in two ways: desiccation cracking and thermal contraction cracking. Thermal contraction cracks are responsible for the V-shaped formation of periglacial sand wedges (Péwé 1959; Lachenbruch 1962; Murton 2013). When heated, most solid materials expand, and when cooled, they contract. Indeed, thermal contraction cracking is thought to be the result of tension caused by permafrost surface.

In winter, cracks form when tensile stresses induced by the cooling of the ground surface and subsurface exceed the tensile strength of the frozen soil (Péwé 1959; Lachenbruch 1962; Maloof *et al*. 2002; Murton 2013). The cracks are vertical, and they taper downwards because horizontal tensile stresses decline with depth (Lachenbruch 1962). Fracture propagation and intersection ultimately result in a polygonal network of vertical or near-vertical cracks penetrating from the surface to depth (Hallet *et al*. 2011). In the process, desiccation cracking may play a strengthening role (Murton *et al*. 2000). Sand veins near sand wedges, formed by cracks that subsequently fill, may reflect an early stage of sand wedge growth (Murton *et al*. 2000). Cracks recur at the same location because previous cracks form lines of weakness (Murton 2013).

5.1.2 Origin of fillings

Periglacial sand wedges typically comprise well-laminated sand that was blown into narrow (mm-sized) thermal contraction cracks in the upper part of permafrost during severe, arid winters (Péwé 1959). Sand grains in wedges indicate greater aeolian abrasion than in host material and are similar to those from aeolian coversand or dunes (Murton *et al*. 2000). Most sands fall into cracks from strong wind. In the filling process, the wind also causes impact and abrasion of grains and forms irregular pits, smooth surfaces, bulbous edges, dish-shaped impact features, crescent-shaped impact scars, etc. on the grain surfaces (Murton *et al*. 2000; Vos *et al*. 2014). Crescentic percussion marks result from severe grain-to-grain collisions (Campbell 1963) and are typical markers of aeolian environments (Vos *et al*. 2014). Bulbous edges, which are prominent, protruding, and rounded grain edges in the shape of a parabolic curve, are attributed to the rotation of saltating grains (Mahaney 2002; Vos *et al*. 2014). The occurrence of dish-shaped features and bulbous edges is diagnostic of aeolian transportation phases (Costa *et al*. 2013).

Some wedges contain vertically layered gravels with desert varnish, which are hard to move by wind but may be dropped by strong wind and slip into cracks during the Gobi periods. Another possibility is that the large grains have been transported into wedges by saltation or as a creeping bedload. These pebbles can only fall into the upper part of the sand wedge because the wedge has a limited crack width. In the process, the limited crack width may act as a filter mechanism restricting the larger grains within the upper part of the crack when the grains fall (Harry and Gozdzik 1988; Murton *et al*. 2000).

The upturning of the host rocks near the shoulder part of the sand wedge is probably due to the blocking of the fillings when the frozen soil warms and expands (Black 1976; Murton *et al*. 2000). This also leads to deformation of the surrounding rock and wedge edges, as full closure is prevented by new debris that enters the cracks (MacKay 2002; Hallet *et al*. 2011). In some cases, sand wedges form arched shoulders when the filling is squeezed (Hallet *et al*. 2011). However, most shoulders flatten and degrade with time (Murton 2013).

Repeated cracking and filling with sand produces wedge-shaped fillings. Therefore, the relict sand wedges in this paper are the result of wedges growing progressively upward at a site of permafrost aggradation, forming syngenetic wedges (MacKay 2002). The vertical to steeply dipping lamination within the wedge is formed by the occurrence of repeated cracking and infilling (Murton *et al*. 2000; Murton 2013). A vertical layer represents one cracking-filling cycle during the sand wedge growth process.

5.2 Periglacial sand wedges grow in cold, arid, windy desert

Cold and arid climates are both important factors in the formation of sand wedges. The ground would not crack if it were not for the cold climate. If the climate gets humid, the cracks can develop into ice wedges. Thus, the rapid cooling of the cold climate dominated the cracking, while the arid climate determined the sand wedge filling. Relict sand wedges indicate the former occurrence of sand transport, often by wind, during winter or spring and little or no snow cover; otherwise, the cracks may fill with ice or ice-sand mixtures (Murton 2000). The traces of sand wedges indicate hyperarid-cold conditions with strong winds (Murton 2013; French 2018). During the Quaternary, most of the actively growing sand wedges were discovered in extremely cold, arid, and ice-free areas of the cryosphere (French 2018). In arid periglacial regions, with <100 mm of mean annual precipitation, the wedges tended to open by thermal contraction cracks at the ground surface and were filled partially

with near-vertically laminated sand by recurrent expansion, wind-blown material infilling, and contraction cycles (Williams 1986).

It must be mentioned that the McMurdo Dry Valleys in Antarctica, the driest place on Earth where the actively growing sand wedges are developed, has mean annual valley floor temperatures ranging from −15 to −30°C (Péwé 1959; Doran *et al*. 2002; Hallet *et al*. 2011). Washburn (1980) concluded that ice and sand wedges suggest a conservative maximum MAAT of −5°C, and sand wedges may indicate colder conditions than ice wedges (Washburn 1980). By comparison, Karte (1983) considered that sand wedges may indicate a MAAT of <-20°C and a mean monthly air temperature range as great as <-35 to +4°C (Karte 1983). The mean air temperature of the coldest month may also reflect the climatic conditions formed by the sand wedge because extreme winter conditions are conducive to thermal contraction cracking (Harry and Gozdzik 1988).

Williams (1986), (2016)) and Ewing *et al*. (2014) proposed that wedge structures provide good evidence for a strongly seasonal paleoclimate, as only the seasonal temperature cycle, coupled with rapid drops in temperature, can produce contraction cracking that leads to wedge formation (Ewing *et al*. 2014; Williams *et al*. 2016). However, Sweet and Soreghan (2008) reported a case of a sand wedge near the equator that formed under a setting of a large temperature difference between day and night in the Permian (Sweet and Soreghan 2008). Obviously, the climatic oscillations of yearly, seasonal, and diurnal variations can also contribute to the formation of sand wedges (Figure 8a). Sand wedge under strongly interannual or seasonal paleoclimate can be distinguished from under diurnal temperature cycle in having relatively deep and large shape, while the latter wedges have small and narrow shape. According to Murton *et al*. (2000), relict primary sand wedges exceeding 2 metres in depth and with well-developed vertical lamination indicate the former presence of continuous permafrost. Based on foregoing, the Ordos Basin relict sand wedges development in continuous permafrost under strongly interannual or seasonal paleoclimate. When sand wedges are preserved, they become the most useful climatic indicators to confirm the existence of undisputed periglacial continuous permafrost or seasonally frozen ground. In particular, relict primary sand wedges >2 m high and with well-developed vertical lamination usually indicate the former occurrence of continuous permafrost because the maximum seasonal frost crack depth is generally less than 2 m (Murton, 2013).

5.3 Implications for the paleoclimate and paleoenvironment in North China

The prevailing view is that temperature conditions increase with altitude and latitude (Manabe and Strickler 1964; Zhang *et al*. 2016). Therefore, two hypotheses could explain the Early Cretaceous arid and cold climate in Ganquan, Ordos Basin, North China at paleolatitudes of ~40°N latitude: (i) As the climate became colder, the cryosphere expanded southward from the Arctic to North China; (ii) The other possibility is that the Ordos Basin, and even North China, uplifted into high landscapes and had a plateau climate because of the collision of adjacent plates.

During most of the Cretaceous period, temperatures of the warmest surface waters were significantly greater than the maximum surface temperatures recorded in the modern ocean (~28-30°C) (Huber *et al*. 2002; Royer *et al*. 2007; Littler *et al*. 2011; Haq 2014; Wang *et al*. 2014; O'Brien *et al*. 2017). However, a variety of findings, including dropstones, tillites, and glauberite-like calcite at various high-latitude locations in the Early Cretaceous, indicate that polar glaciers existed (e.g. Alley and Frakes 2003; Frakes and Francis 1988; Frakes *et al*. 1995; Price 1999; Kuhnt *et al*. 2011). The occurrence of cooler episodes and/or ephemeral ice sheets at times in the Cretaceous has been proposed and debated by geologists (Alley and Frakes, 2003; Frakes and Francis 1988; Frakes *et al*. 1995; Price 1999; Kuhnt *et al*. 2011). The scale and intensity of polar glaciers in the Early Cretaceous may be smaller than modern glaciers (Alley and Frakes 2003; Eriksson *et al*. 2013). That is to say, these polar cryospheres appear to be too small to accommodate the geological phenomenon of periglacial sand wedges growing in low-elevation continental areas at ~30-40°N latitude (Ma *et al*. 1993; Huang *et al*. 2008). In paleotemperature reconstructions, the global average temperature during the Early Cretaceous fluctuated between 18°C and 24°C (Scotese *et al*. 2021). The modern global average temperature is 14.5°C. Today permafrost exists at low latitudes (e.g. ~35°N in Qinghai-Tibet Plateau), but only at very high altitudes (>~4.5–5.0 km), so middle-latitude permafrost in the Early Cretaceous would need to have been at high elevation to reveal a climate warmer than the today's climate.

The strongest possibility is that Early Cretaceous sand wedges were active on highlands, such as the present-day Qinghai-Tibet Plateau, where the average altitude exceeds 4000 m. In North China, an angular unconformity beneath the Lower Cretaceous registered this contractional event called Phase B of the Yanshanian

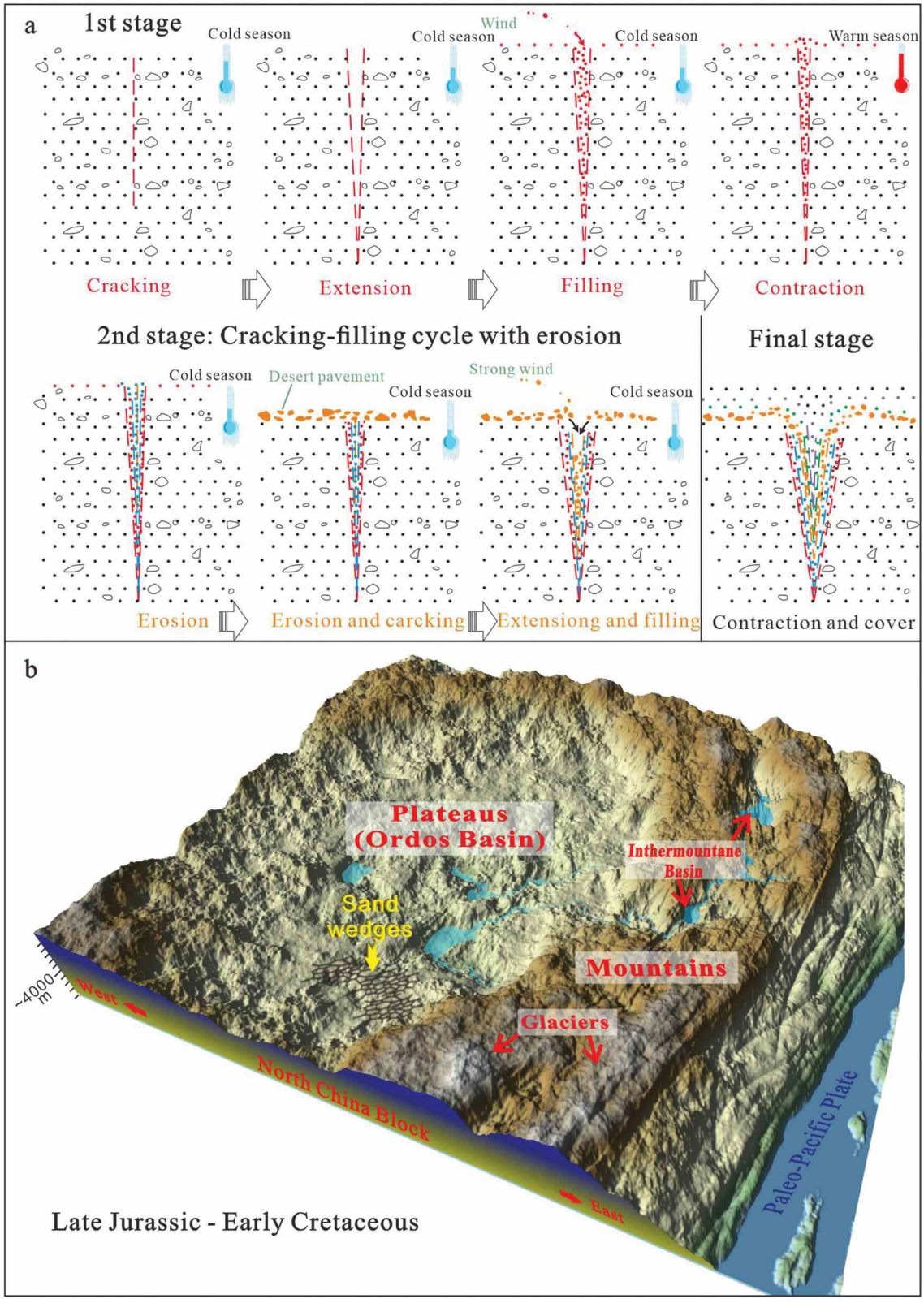

Figure 8. (a) Schematic vertical section showing the growth process and ultimate form of the sand wedge. (b) Conjectural reconstruction of paleo-landform of the sand wedges in North China. The elevation were only estimated crudely.

orogeny, may have been triggered by subduction of the Paleo-Pacific plate beneath the Asian continent (Zhu *et al*. 2017). During the early Early Cretaceous Yanshanian orogeny's Phase B compression, a series of massive folds and thrust belts were developed on the outskirts of the Ordos Basin. Apatite fission track data from the Ordos Basin's western side indicate that the Helan mountain was uplifted and denuded during the Late Jurassic-Early Cretaceous period (Zhao *et al*. 2007). The thermochronology of the southwest margin of Ordos Basin also reveals that the rapid uplifting event occurred in the Late Jurassic-Early Cretaceous (170-130 Ma) (Peng *et al*. 2022). In the Helan mountain area, there is a high angle unconformity between Lower Cretaceous and Jurassic strata in the Helan Mountain area. In the outcrop and seismic section, strong deformation occurred in the Jurassic Yan'an Formation and weak deformation occurred in the Lower Cretaceous Zhidan Group, indicating that a large scale thrust nappe and tectonic uplift occurred in the Late Jurassic-Early Cretaceous. Combined with the distribution of the conglomerate in the Huanxian-Qianyang area, it indicates that the tectonic uplift may have affected the inner Ordos Basin (Zhao *et al*. 2020b). In the Early Cretaceous, the Qinling Orogenic Belt and adjacent areas on the southern side of the Ordos Basin were rapidly uplifted and exhumed (Dong *et al*. 2011; Chen *et al*. 2015). The Yanshanian orogenic event plays a major role for rapid exhumation of significant portions of the Early Cretaceous Qinling Orogenic Belt (Dong *et al*. 2011). During the Late Jurassic-Early Cretaceous (~161-139 Ma), the Yinshan Orogenic Belt in the northern margin of the Ordos Basin, also the northern margin of North China, formed the giant fold and thrust belt (belonging to the Central Asian Orogenic Belt), and synorogenic coarse-grained sediments were deposited in these areas (Liu *et al*. 2015; Yang *et al*. 2015). At the same time, Yanshanian orogenic event may have led to the uplift in the Luliang Mountain area on the eastern side of the Ordos Basin (Clinkscales and Kapp 2019; Zhang *et al*. 2022). Furthermore, several recent plate tectonics studies have suggested that during the late Mesozoic, the eastern part of North China was probably in a high plateau region with a scale and elevation similar to the present-day Qinghai-Tibet Plateau (Deng *et al*. 2000; Zhang *et al*. 2008; Xia *et al*. 2012).

The plate tectonic motioned to crustal uplift and the climate cooling. Moreover, highlands (plateaus or mountains) block water vapour transmission and cause drought (Rahbek *et al*. 2019). Plateaus at low latitudes with large day-night temperature differences can also provide necessary climatic conditions for the activity of sand wedges. According to the modern atmospheric pressure and climate, the average elevation of the Ordos Basin was higher than 3600 m when the sand wedges were actively growing in Early Cretaceous (Manabe and Strickler 1964; Cess 1976; Hay 2008; Littler *et al*. 2011). Evidence from plants, sporopollens, isotopes of dinosaur bones, and other evidences (Li *et al*. 2008; Philippe *et al*. 2009, 2013; Amiot *et al*. 2011; Ding *et al*. 2016; Wang *et al*. 2017; Zhang *et al*. 2021) also support our view that the waxing and waning of a climate and the existence of possible mountains or plateaus in North China during the Late Jurassic-Early Cretaceous (Figure 1d; Figure 8b).

Interestingly, the famous Jehol Biota flourished in the mountains and lakes of northeast China during the Early Cretaceous (Zhou 2014; Xu *et al*. 2020). Jehol Biota biomolecules have also been found in the areas such as the Yin'e Basin of western North China (Zhang *et al*. 2022). The mixed phenomenon of a few cold-loving molecular spores and pollen such as spruce, cedar and fir with tropical and subtropical spores and pollen suggest vertical zoning of plants and the paleoclimate (Zhang *et al*. 2022). Along with the forementioned phenomena, the sand wedges were deposited in a cold, dry climate and were inferred to be periglacial sedimentary structures in the Ordos Basin, implying a topographically complex North China with diverse climate types.

6. Conclusion

In this study, the characteristics of relict sand wedges in Ganquan in the Ordos Basin during the Late Jurassic-Early Cretaceous are described. The relict sand wedges, interpreted as the result of thermal contraction cracking by waxing and waning a cold climate, are some of the most convincing evidence for permafrost. It is a unique cold, arid, and windy marker and indicates that the Ordos Basin was within the cryosphere zone and was a periglacial desert. The expressions of periglacial sand wedges may be attributable to Late Jurassic-Early Cretaceous highlands (>3600 m altitude) that generated surface uplift coupled with a temperature drop. The relict sand wedges in this study contribute to an in-depth understanding of the paleoclimate, paleoenvironment and palaeoecology in North China during the period when the Jehol Biota existed.

Acknowledgments

This work was supported by the Natural Science Foundation of China [grant number 41688103, 42072135], China Geological Survey [grant number DD20221649, DD20190005]. We

appreciate the helpful comments and suggestions from the two anonymous reviewers.

Disclosure statement

No potential conflict of interest was reported by the author(s).

Funding

This work was supported by the China Geological Survey [DD20190005,DD20221649]; National Natural Science Foundation of China [41688103,42072135].

ORCID

Yuchong Wang http://orcid.org/0000-0003-2226-9919
Nan Peng http://orcid.org/0000-0003-2355-3188
Hongwei Kuang http://orcid.org/0000-0003-3649-8763
Fenghua Zhao http://orcid.org/0000-0001-5935-8371
Yongqing Liu http://orcid.org/0000-0002-9131-0172

Highlights

The first report of relict sand wedges by thermal contraction cracking at the bottom of the Cretaceous strata.

The Ordos Basin, western North China, was under cold, arid, and windy permafrost conditions in the Early Cretaceous.

The Ordos Basin may have been at a high altitude and was cold during the Early Cretaceous.

References

Allen, J.R.L., 1982. Sedimentary structures, their character and physical basis, developments in sedimentology. Elsevier Scientific Pub. Co, Amsterdam; New York. pp.343–393.

Alley, N.F., and Frakes, L.A., 2003. First known cretaceous glaciation: Livingston tillite member of the cadna-owie formation, South Australia. Australian Journal of Earth Sciences 50, 139–144. doi: 10.1046/j.1440-0952.2003.00984.x 2

Amiot, R., Wang, X., Zhou, Z., Wang, X., Buffetaut, E., Lecuyer, C., Ding, Z., Fluteau, F., Hibino, T., Kusuhashi, N., Mo, J., Suteethorn, V., Wang, Y., Xu, X., and Zhang, F., 2011. Oxygen isotopes of East Asian dinosaurs reveal exceptionally cold early Cretaceous climates. Proceedings of the National Academy of Sciences 108, 5179–5183. doi: 10.1073/pnas.1011369108.

Andrieux, E., Bateman, M.D., and Bertran, P., 2018. The chronology of late Pleistocene thermal contraction cracking derived from sand wedge OSL dating in central and southern France. Global and Planetary Change 162, 84–100. doi: 10.1016/j.gloplacha.2018.01.012

Bateman, M.D., Evans, D.J.A., Buckland, P.C., Connell, E.R., Friend, R.J., Hartmann, D., Moxon, H., Fairburn, W.A., Panagiotakopulu, E., and Ashurst, R.A., 2015. Last glacial dynamics of the Vale of York and North Sea lobes of the British and Irish Ice Sheet. Proceedings of the Geologists' Association. 126, 712–730. doi: 10.1016/j.pgeola.2015.09.005

Black, R.F., 1976. Periglacial features indicative of permafrost: ice and soil wedges. Quat. Res. 6, 3–26. doi: 10.1016/0033-5894(76)90037-5 1

Black, R.F., 1983. Pseudo-ice-wedge casts of Connecticut, northeastern United States. Quaternary Research 20, 74–89. doi: 10.1016/0033-5894(83)90066-2 1

Burbidge, G.H., French, H.M., and Rust, B.R., 2008. Water escape fissures resembling ice-wedge casts in late quaternay subaqueous outwash near St. Lazare Québec, Canada. Boreas 17, 33–40. doi: 10.1111/j.1502-3885.1988.tb00122.x 1

Campbell, D.H., 1963. Percussion marks on quartz grains. Journal of Sedimentary Research 33, 855–859. doi: 10.1306/74D70F60-2B21-11D7-8648000102C1865D

Cess, R.D., 1976. Climate change: An appraisal of atmospheric feedback mechanisms employing zonal climatology. Journal of the Atmospheric Sciences 33, 1831–1843. doi:10.1175/1520-0469(1976)033<1831:CCAAOA>2.0.CO;2>

Chen, H., Hu, J., Wu, G., Shi, W., Geng, Y., and Qu, H., 2015. Apatite fission-track thermochronological constraints on the pattern of late Mesozoic–Cenozoic uplift and exhumation of the Qinling Orogen, central China. Journal of Asian Earth Sciences, Mesozoic Lithospheric Structures and Tectonic Development of East Asia 114, 649–673. doi: 10.1016/j.jseaes.2014.10.004

Cheng, S.T., Li, Z.D., Huang, Y.Q., Ge, L., and Liu, X., 2002. Discovery and its genetic evidences of early cretaceous glacial debris flow in the northeast margin of Ordos. Geological Science and Technology Information 21, 36–40 (in Chinese with English abstract).

Clemmensen, L.B., and Tirsgaard, H., 1990. Sand-drift surfaces: A neglected type of bounding surface. Geology 18, 1142–1145. 11 doi: 10.1130/0091-7613(1990)018<1142:SDSANT>2.3.CO;2

Clinkscales, C., and Kapp, P., 2019. Structural style and kinematics of the Taihang-Luliangshan fold belt, North China: implications for the Yanshanian orogeny. Lithosphere 11, 767–783. doi: 10.1130/L1096.1 6

Costa, P.J.M., Andrade, C., Mahaney, W.C., Marques da Silva, F., Freire, P., Freitas, M.C., Janardo, C., Oliveira, M.A., Silva, T., and Lopes, V., 2013. Aeolian microtextures in silica spheres induced in a wind tunnel experiment: Comparison with aeolian quartz. Geomorphology 180-181, 120–129. doi: 10.1016/j.geomorph.2012.09.011

Darby, B.J., and Ritts, B.D., 2002. Mesozoic contractional deformation in the middle of the Asian tectonic collage: The intraplate Western Ordos fold–thrust belt, China. Earth and Planetary Science Letters 205, 13–24. doi: 10.1016/S0012-821X(02)01026-9 1–2

Deng, J.F., Zhao, G.C., Zhao, H.L., Luo, Z.H., Dai, S.Q., and Li, K.M., 2000. Yanshanian igneous petrotectonic assemblage and orogenic-deep processes in East China. Geological Review 46, 41–48 (in Chinese with English abstract).

Ding, Q., Tian, N., Wang, Y., Jiang, Z., Chen, S., Wang, D., Zhang, W., Zheng, S., Xie, A., Zhang, G., and Liu, Z., 2016. Fossil coniferous wood from the Early Cretaceous Jehol Biota in western Liaoning, NE China: New material and palaeoclimate implications. Cretaceous Research 61, 57–70. doi: 10.1016/j.cretres.2015.12.011

Dong, Y., Zhang, G., Neubauer, F., Liu, X., Genser, J., and Hauzenberger, C., 2011. Tectonic evolution of the Qinling orogen, China: Review and synthesis. Journal of Asian Earth Sciences 41, 213–237. doi: 10.1016/j.jseaes.2011.03.002 3

Doran, P.T., McKay, C.P., Clow, G.D., Dana, G.L., Fountain, A.G., Nylen, T., and Lyons, W.B., 2002. Valley floor climate observations from the McMurdo dry valleys, Antarctica, 1986–2000. Journal of Geophysical Research: Atmospheres 107, ACL 13–1. doi: 10.1029/2001JD002045 D24

Dorn, R.I., and Oberlander, T.M., 1981. Microbial origin of desert varnish. Science 213, 1245–1247. doi: 10.1126/science.213.4513.1245 4513

Enkin, R.J., Yang, Z., Chen, Y., and Courtillot, V., 1992. Paleomagnetic constraints on the geodynamic history of the major blocks of China from the Permian to the present. J. Geophys. Res. 97, 13953. doi: 10.1029/92JB00648 B10

Eriksson, P.G., Banerjee, S., Catuneanu, O., Corcoran, P.L., Eriksson, K.A., Hiatt, E.E., Laflamme, M., Lenhardt, N., Long, D.G.F., Miall, A.D., Mints, M.V., Pufahl, P.K., Sarkar, S., Simpson, E.L., and Williams, G.E., 2013. Secular changes in sedimentation systems and sequence stratigraphy. Gondwana Research 24, 468–489. doi: 10.1016/j.gr.2012.09.008

Ewing, R.C., Eisenman, I., Lamb, M.P., Poppick, L., Maloof, A.C., and Fischer, W.W., 2014. New constraints on equatorial temperatures during a late neoproterozoic snowball earth glaciation. Earth and Planetary Science Letters 406, 110–122. doi: 10.1016/j.epsl.2014.09.017

Fábián, S., Kovács, J., Tarnocai, C., and Varga, G., 2009. Similarities between the recent permafrost in northwestern Canada and the pleistocene relict cryogenic forms in central Europe (Hungary), New permafrost and glacier research. Krugger, M.I., Stern, H.P. Nova Science Publishers, Hauppauge, NY, pp. 107–129.

Fábián, S., Kovács, J., Tarnocai, C., and Varga, G., 2009, Similarities between the recent permafrost in north-western canada and the pleistocene relict cryogenic forms in central europe (Hungary), in Krugger, M.I. and Stern, H.P. eds., New permafrost and glacier research, Hauppauge, NY, Nova Science Publishers, p. 107–129.

Fisher, T.G., 1996. Sand-wedge and ventifact palaeoenvironmental indicators in North-West Saskatchewan, Canada, 11 ka to 9.9 ka BP. Permafrost and Periglacial Processes 7, 391–408. doi: 10.1002/(SICI)1099-1530(199610)7:4<391::AID-PPP229>3.0.CO;2-W 4

Frakes, L.A., and Francis, J.E., 1988. A guide to Phanerozoic cold polar climates from high-latitude ice-rafting in the Cretaceous. Nature 333, 547–549. doi: 10.1038/333547a0 6173

Frakes, L.A., Alley, N.F., and Deynoux, M., 1995. Early Cretaceous ice rafting and climate zonation in Australia. International Geology Review 37, 567–583. doi: 10.1080/00206819509465419 7

French, H.M., 2018. The periglacial environment, Fourth edition. ed. Wiley Blackwell, Hoboken, NJ.

Goldsmith, Y., Stein, M., and Enzel, Y., 2014. From dust to varnish: Geochemical constraints on rock varnish formation in the Negev Desert, Israel. Geochimica et Cosmochimica Acta 126, 97–111. doi: 10.1016/j.gca.2013.10.040

Hallet, B., Sletten, R., and Whilden, K., 2011. Micro-relief development in polygonal patterned ground in the Dry Valleys of Antarctica. Quaternary Research 75, 347–355. doi: 10.1016/j.yqres.2010.12.009 2

Haq, B.U., 2014. Cretaceous eustasy revisited. Global and Planetary Change 113, 44–58. doi: 10.1016/j.gloplacha.2013.12.007

Harry, D.G., and Gozdzik, J.S., 1988. Ice wedges: Growth, thaw transformation, and palaeoenvironmental significance. J. Quaternary Sci. 3, 39–55. doi: 10.1002/jqs.3390030107 1

Hay, W.W., 2008. Evolving ideas about the Cretaceous climate and ocean circulation. Cretaceous Research 29, 725–753. doi: 10.1016/j.cretres.2008.05.025

Huang, B.C., Zhou, Y.X., and Zhu, R.X., 2008. Discussions on Phanerozoic evolution and formation of continental China, based on paleomagnetic studies. Earth Science Frontiers 15, 348–359 (in Chinese with English abstract).

Huang, Y., 2010. The origin and evolution of the desert in southern Ordos in Early Cretaceous: Constraint from magnetostratigraphy of Zhidan Group and magnetic susceptibility of its sediment [Maser's thesis]: Lanzhou, University, Lanzhou, 78 p. (in Chinese with English abstract).

Huber, B.T., Norris, R.D., and MacLeod, K.G., 2002. Deep-sea paleotemperature record of extreme warmth during the Cretaceous. Geology 30, 123–126. 2 doi: 10.1130/0091-7613-(2002)030<0123:DSPROE>2.0.CO;2

Hunter, R.E., 1977. Basic types of stratification in small eolian dunes. Sedimentology 24, 361–387. doi: 10.1111/j.1365-3091.1977.tb00128.x 3

Jiang, X., Pan, Z., and Fu, Q., 2001. Regularity of paleowind directions of the Early Cretaceous Desert in Ordos Basin and climatic significance. Science in China Series D-Earth Sciences 44, 24–33. doi: 10.1007/BF02906882 1

Jin, H.J., Chang, X.L., and Wang, S.L., 2007. Evolution of permafrost on the Qinghai-Xizang (Tibet) Plateau since the end of the late Pleistocene. J. Geophys. Res. 112, F02S09. doi: 10.1029/2006JF000521

Karte, J., 1983. Periglacial phenomena and their significance as climatic and edaphic indicators. GeoJournal 7, 329–340. doi: 10.1007/BF00241455 4

Kocurek, G., and Hunter, R.E., 1986. Origin of polygonal fractures in sand, uppermost Navajo and Page sandstones, Page, Arizona. Journal of Sedimentary Research 56, 895–904. doi: 10.1306/212F8A7B-2B24-11D7-8648000102C1865D

Kraus, M.J., and Gwinn, B., 1997.Facies and facies architecture of Paleogene floodplain deposits, Willwood Formation, Bighorn Basin, Wyoming, USA . Sedimentary Geology 114, 33–54. doi: 10.1016/S0037-0738(97)00083-3

Krinsley, D.H., Friend, P.F., and Klimentidis, R., 1976. Eolian transport textures on the surfaces of sand grains of Early Triassic age. GSA Bulletin 87, 130–132. 1 doi: 10.1130/0016-7606(1976)87<130:ETTOTS>2.0.CO;2

Kuhnt, W., Holbourn, A., and Moullade, M., 2011. Transient global cooling at the onset of early Aptian oceanic anoxic event (OAE) 1a. Geology 39, 323–326. doi: 10.1130/G31554.1 4

Lachenbruch, A.H., 1962. Mechanics of thermal contraction cracks and ice-wedge polygons in permafrost, in: Geological Society of America Special Papers. Geological Society of America, pp. 1–66. doi: 10.1130/SPE70-p1

Li, X.H., Xu, B.L., Chen, Y.H., Cao, K., and Yang, H., 2008. Clay minerals of the middle-late mesozoic mudrocks from North and Northeast China: Implications to paleoclimate and paleohighland. Acta Geologica Sinica 82, 683–691 (in Chinese with English abstract).

Li, H., Wang, W., Wu, F., Zhan, H., Zhang, G., and Qiu, F., 2014. A new sand-wedge–forming mechanism in an extra-arid area. Geomorphology 211, 43–51. doi: 10.1016/j.geomorph.2013.12.028

Li, Z., Dong, S., Feng, S., and Qu, H., 2015. Sedimentary response to middle-late Jurassic tectonic events in the Ordos Basin. Acta Geoscientica Sinica 21–29. doi: 10.3975/cagsb.2015.01.03

Li, G., 2017. SEM morphological study of the type species of Ordosestheria Wang, 1984 (Spinicaudata) from Ordos Basin of mid-west China. Cretaceous Research 75, 1–6. doi: 10.1016/j.cretres.2017.03.006

Littler, K., Robinson, S.A., Bown, P.R., Nederbragt, A.J., and Pancost, R.D., 2011. High sea-surface temperatures during the early cretaceous epoch. Nature Geoscience 4, 169–172. doi: 10.1038/ngeo1081 3

Liu, Y., Kuang, H., Peng, N., Xu, H., Zhang, P., Wang, N., An, W., Wang, Y., Liu, M., and Hu, X., 2015. Mesozoic basins and associated palaeogeographic evolution in North China. Journal of Palaeogeography 4, 189–202. doi: 10.3724/SP.J.1261.2015.00073 2

Loope, D.B., and Haverland, Z.E., 1988. Giant desiccation fissures filled with calcareous eolian sand, hermosa formation (Pennsylvanian), southeastern Utah. Sedimentary Geology 56, 403–413. doi: 10.1016/0037-0738(88)90063-2 1–4

Ma, X., Xing, L., Yang, Z., Xu, S., and Zhang, J., 1993. Paleomagnetic study since late Paleozoic in the Ordos basin. Chinese Journal of Geophysics 36, 68–79 (in Chinese with English abstract).

MacKay, J.R., 2002. Thermally induced movements in ice-wedge polygons, western Arctic coast: A long-term study. Gpq 54, 41–68. doi: 10.7202/004846ar 1

Mahaney, W.C., 2002. Atlas of sand grain surface textures and applications. Oxford University Press, Oxford ; New York.

Maloof, A.C., Kellogg, J.B., and Anders, A.M., 2002. Neoproterozoic sand wedges: Crack formation in frozen soils under diurnal forcing during a snowball Earth. Earth and Planetary Science Letters 204, 1–15. doi: 10.1016/S0012-821X(02)00960-3 1–2

Manabe, S., and Strickler, R.F., 1964. Thermal equilibrium of the atmosphere with a convective adjustment. Journal of Atmospheric Sciences 21, 361–385. 4 doi: 10.1175/1520-0469(1964)021<0361:TEOTAW>2.0.CO;2

Matmon, A., Simhai, O., Amit, R., Haviv, I., Porat, N., McDonald, E., Benedetti, L., and Finkel, R., 2009. Desert pavement-coated surfaces in extreme deserts present the longest-lived landforms on Earth. Geological Society of America Bulletin 121, 688–697. doi: 10.1130/B26422.1 5–6

McFadden, L.D., Wells, S.G., and Jercinovich, M.J., 1987. Influences of eolian and pedogenic processes on the origin and evolution of desert pavements. Geology 15, 504–508. 6 doi: 10.1130/0091-7613(1987)15<504:IOEAPP>2.0.CO;2

Mellon, M.T., Mckay, C.P., and Heldmann, J.L., 2014. Polygonal ground in the McMurdo dry valleys of Antarctica and its relationship to ice-table depth and the recent Antarctic climate history. Antarctic Science 26, 413–426. doi: 10.1017/S0954102013000710 4

Meng, Q.-R., Wu, G.-L., Fan, L.-G., and Wei, -H.-H., 2019. Tectonic evolution of early Mesozoic sedimentary basins in the North China block. Earth-Science Reviews 190, 416–438. doi: 10.1016/j.earscirev.2018.12.003

Moretti, M., and Sabato, L., 2007. Recognition of trigger mechanisms for soft-sediment deformation in the Pleistocene lacustrine deposits of the Sant'Arcangelo Basin (Southern Italy): Seismic shock vs. overloading. Sedimentary Geology, Deformation of Soft Sediments in Nature and Laboratory 196, 31–45. doi: 10.1016/j.sedgeo.2006.05.012

Murton, J.B., Worsley, P., and Gozdzik, J., 2000. Sand veins and wedges in cold aeolian environments. Quaternary Science Reviews 19, 899–922. doi: 10.1016/S0277-3791(99)00045-1 9

Murton, J., 2013. Permafrost and periglacial features | ice wedges and ice-wedge casts, in Elias, S.A. and Mock, C.J. eds., Encyclopedia of Quaternary Science, Amsterdam, Elsevier, p. 436–451. doi:10.1016/B978-0-444-53643-3.00097-2.

O'Brien, C.L., Robinson, S.A., Pancost, R.D., Sinninghe Damsté, J.S., Schouten, S., Lunt, D.J., Alsenz, H., Bornemann, A., Bottini, C., Brassell, S.C., Farnsworth, A., Forster, A., Huber, B.T., Inglis, G.N., Jenkyns, H.C., Linnert, C., Littler, K., Markwick, P., McAnena, A., Mutterlose, J., Naafs, B.D.A., Püttmann, W., Sluijs, A., van Helmond, N.A.G.M., Vellekoop, J., Wagner, T., and Wrobel, N.E., 2017. Cretaceous sea-surface temperature evolution: Constraints from TEX 86 and planktonic foraminiferal oxygen isotopes. Earth-Science Reviews 172, 224–247. doi: 10.1016/j.earscirev.2017.07.012

Owen, G., and Moretti, M., 2011. Identifying triggers for liquefaction-induced soft-sediment deformation in sands. Sedimentary Geology 235, 141–147. doi: 10.1016/j.sedgeo.2010.10.003 3–4

Øygarden, L., 2003. Rill and gully development during an extreme winter runoff event in Norway. CATENA, Gully Erosion and Global Change 50, 217–242. doi: 10.1016/S0341-8162(02)00138-8

Peng, H., Liu, C., Hui, X., Quan, X., Zhang, T., Zhao, H., and Wang, J., 2022. Spatial- temporal evolution and the dynamic background of the translation of Mid- Late Mesozoic tectonic regimes of the southwest Ordos basin margin. Acta Geologica Sinica 96, 387–402 (in Chinese with English abstract).

Perry, R.S., Lynne, B.Y., Sephton, M.A., Kolb, V.M., Perry, C.C., and Staley, J.T., 2006. Baking black opal in the desert sun: The importance of silica in desert varnish. Geology 34, 537–540. doi: 10.1130/G22352.1 7

Péwé, T.L., 1959. Sand-wedge polygons (tesselations) in the McMurdo Sound region, Antarctica; a progress report. Am J Sci 257, 545. doi: 10.2475/ajs.257.8.545 8

Philippe, M., JIANG, H., Kim, K., Oh, C., Gromyko, D., Harland, M., Paik, I., and Thevenard, F., 2009. Structure and diversity of the Mesozoic wood genusXenoxylonin Far East Asia: Implications for terrestrial palaeoclimates. Lethaia 42, 393–406. doi: 10.1111/j.1502-3931.2009.00160.x 4

Philippe, M., Thévenard, F., Nosova, N., Kim, K., and Naugolnykh, S., 2013. Systematics of a palaeoecologically significant boreal Mesozoic fossil wood genus, Xenoxylon Gothan. Review of Palaeobotany and Palynology 193, 128–140. doi: 10.1016/j.revpalbo.2013.01.013

Price, G.D., 1999. The evidence and implications of polar ice during the Mesozoic. Earth-Science Reviews 48, 183–210. doi: 10.1016/S0012-8252(99)00048-3 3

Qiao, D., Kuang, H., Liu, Y., Peng, N., Liu, Y., Xu, H., Cui, L., and Li, Z., 2020. Identification of eolian sandstone in Cretaceous uraniferous sandstone in Ordos Basin, China. Geotectonica Et Metallogenia 44, 648–666. doi: 10.16539/j.ddgzyckx.2020.04.008

Qiao, D., Peng, N., Kuang, H., Liu, Y., Liu, Y., Cui, L., and Wang, Y., 2022. Changes in prevailing surface-paleowinds reveal the atmospheric circulation transition during Early Cretaceous in North China. Palaeogeography, Palaeoclimatology, Palaeoecology 586, 110784. doi: 10.1016/j.palaeo.2021.110784

Rahbek, C., Borregaard, M.K., Colwell, R.K., Dalsgaard, B., Holt, B.G., Morueta-Holme, N., Nogues-Bravo, D., Whittaker, R.J., and Fjeldså, J., 2019. Humboldt's enigma: What causes global patterns of mountain biodiversity? Science 365, 1108–1113. doi: 10.1126/science.aax0149 6458

Rogov, M.A., Ershova, V.B., Shchepetova, E.V., Zakharov, V. A., Pokrovsky, B.G., and Khudoley, A.K., 2017. Earliest Cretaceous (late Berriasian) glendonites from Northeast Siberia revise the timing of initiation of transient Early Cretaceous cooling in the high latitudes. Cretaceous Research 71, 102–112. doi: 10.1016/j.cretres.2016.11.011

Royer, D.L., Berner, R.A., and Park, J., 2007. Climate sensitivity constrained by CO 2 concentrations over the past 420 million years. Nature 446, 530–532. doi: 10.1038/nature05699 7135

Scherer, C.M.S., Lavina, E.L.C., Dias Filho, D.C., Oliveira, F.M., Bongiolo, D.E., and Aguiar, E.S., 2007. Stratigraphy and facies architecture of the fluvial–aeolian–lacustrine Sergi Formation (Upper Jurassic), Recôncavo Basin, Brazil. Sedimentary Geology 194, 169–193. doi: 10.1016/j.sedgeo.2006.06.002 3–4

Scotese, C.R., Song, H., Mills, B.J.W., and van der Meer, D. G., 2021. Phanerozoic paleotemperatures: The earth's changing climate during the last 540 million years. Earth-Science Reviews 215, 103503. doi: 10.1016/j.earscirev.2021.103503

Shen, Y., Zhang, C., Wang, R., Wang, X., Cen, S., and Li, Q., 2020. Spatial heterogeneity of surface sediment grain size and aeolian activity in the gobi desert region of northwest China. CATENA 188, 104469. doi: 10.1016/j.catena.2020.104469

Sweet, D.E., and Soreghan, G.S., 2008. Polygonal cracking in coarse clastics records cold temperatures in the equatorial fountain formation (Pennsylvanian–Permian, Colorado). Palaeogeography, Palaeoclimatology, Palaeoecology 268, 193–204. doi: 10.1016/j.palaeo.2008.03.046 3–4

Thiagarajan, N., and Aeolus Lee, C.-T., 2004. Trace-element evidence for the origin of desert varnish by direct aqueous atmospheric deposition. Earth and Planetary Science Letters 224, 131–141. doi: 10.1016/j.epsl.2004.04.038 1–2

Velde, B., 1999. Structure of surface cracks in soil and muds. Geoderma 93, 101–124. doi: 10.1016/S0016-7061(99)00047-6 1–2

Vos, K., Vandenberghe, N., and Elsen, J., 2014. Surface textural analysis of quartz grains by scanning electron microscopy (SEM): From sample preparation to environmental interpretation. Earth-Science Reviews 128, 93–104. doi: 10.1016/j.earscirev.2013.10.013

Wang, S., 1984. New Jurassic-Cretaceous conchostracans from northern Hebei and nei mongol. Acta Palaeontologica Sinica 6, 726–737+802–804. doi: 10.19800/j.cnki.aps.1984.06.007

Wang, D.P., Liu, L., and Frakes, L.A., 1996. The palaeoclimatic and palaeogeographic significance of the Cretaceous red-bed icerafting deposits in the Songliao Basin, northeastern China. Sedimentary Facies and Palaeogeography 16, 6–11 (in Chinese with English abstract).

Wang, Y., Huang, C., Sun, B., Quan, C., Wu, J., and Lin, Z., 2014. Paleo-CO2 variation trends and the Cretaceous greenhouse climate. Earth-Science Reviews 129, 136–147. doi: 10.1016/j.earscirev.2013.11.001

Wang, Y., Tian, N., Jiang, Z., Yang, X., and Ding, Q., 2017. Recent advances in Mesozoic fossil wood studies in China: Diversity variations and palaeoclimate implications. Earth Sciences Frontiers 24, 52–64. doi: 10.13745/j.esf.2017.01.004

Washburn, A.L., 1980. Permafrost features as evidence of climatic change. Earth-Science Reviews 15, 327–402. doi: 10.1016/0012-8252(80)90114-2 4

Watanabe, T., Matsuoka, N., and Christiansen, H.H., 2013. Ice- and soil-wedge dynamics in the Kapp Linné Area, Svalbard, investigated by two- and three-dimensional GPR and ground thermal and acceleration regimes. Permafrost and Periglac. Process. 24, 39–55. doi: 10.1002/ppp.1767 1

Weinberger, R., 2001. Evolution of polygonal patterns in stratified mud during desiccation: The role of flaw distribution and layer boundaries. GSA Bulletin 113, 20–31. 1 doi: 10.1130/0016-7606(2001)113<0020:EOPPIS>2.0.CO;2

Williams, G.E., 1986. Precambrian permafrost horizons as indicators of palaeoclimate. Precambrian Research 32, 233–242. doi: 10.1016/0301-9268(86)90008-2

Williams, G.E., Schmidt, P.W., and Young, G.M., 2016. Strongly seasonal Proterozoic glacial climate in low palaeolatitudes: Radically different climate system on the pre-Ediacaran Earth. Geoscience Frontiers 7, 555–571. doi: 10.1016/j.gsf.2016.01.005 4

Xi, D., Wan, X., Guobiao, L., and Li, G. 2019. Cretaceous integrative stratigraphy and timescale of China. Sci. China Earth Sci. 62, 256–286. doi: 10.1007/s11430-017-9262-y

Xia, G., Yi, H., Zhao, X., Gong, D., and Ji, C., 2012. A late Mesozoic high plateau in eastern China: Evidence from basalt vesicular paleoaltimetry. Chin. Sci. Bull. 57, 2767–2777. doi: 10.1007/s11434-012-5169-0 21

Xu, H., Liu, Y., Kuang, H., and Peng, N., 2019. Late Jurassic fluvial–eolian deposits from the tianchihe formation, Ningwu–Jingle Basin, Shanxi Province, China. Journal of Asian Earth Sciences 174, 245–262. doi: 10.1016/j.jseaes.2018.12.012

Xu, X., Zhou, Z., Wang, Y., and Wang, M., 2020. Study on the Jehol Biota: Recent advances and future prospects. Sci. China Earth Sci. 63, 757–773. doi: 10.1007/s11430-019-9509-3 6

Yang, Y., Guo, Z., Song, C., Li, X., and He, S., 2015. A short-lived but significant Mongol–Okhotsk collisional orogeny in latest Jurassic–earliest Cretaceous. Gondwana Research 28, 1096–1116. doi: 10.1016/j.gr.2014.09.010 3

Zhai, M., 2011. Cratonization and the Ancient North China Continent: A summary and review. Sci. China Earth Sci. 54, 1110–1120. doi: 10.1007/s11430-011-4250-x 8

Zhang, Q., Wang, Y.L., Jin, W.J., and Li, C.D., 2008. Eastern China Plateau during the Late Mesozoic: Evidence, problems and implication. Geological Bulletin of China 27, 1404–1430 (in Chinese with English abstract).

Zhang, L., Wang, C., Cao, K., Wang, Q., Tan, J., and Gao, Y., 2016. High elevation of Jiaolai Basin during the Late Cretaceous: Implication for the coastal mountains along the East Asian margin. Earth and Planetary Science Letters 456, 112–123. doi: 10.1016/j.epsl.2016.09.034

Zhang, B., Zhang, J., Zhao, H., Nie, F., Wang, Y., and Zhang, Y., 2019. Tectonic evolution of the western Ordos Basin during the Palaeozoic-Mesozoic time as constrained by detrital zircon ages. International Geology Review 61, 461–480. doi: 10.1080/00206814.2018.1431963 4

Zhang, L., Yin, Y., and Wang, C., 2021. High-altitude and cold habitat for the Early Cretaceous feathered dinosaurs at Sihetun, Western Liaoning, China. Geophysical Research Letters 48, e2021GL094370. doi: 10.1029/2021GL094370

Zhang, Y., Qiu, E., Dong, S., Li, J., and Shi, W., 2022. Late Mesozoic intracontinental deformation and magmatism in North and NE China in response to multi-plate convergence in NE Asia: An overview and new view. Tectonophysics 229377. doi: 10.1016/j.tecto.2022.229377

Zhao, J., Liu, C., Yu, L., Liang, J., and Huang, L., 2006. Sedimentary tectonic features of Ordos basin in Middle Jurassic Zhiluo-Anding stages. Oil & Gas Geology 2, 159–166 (in Chinese with English abstract).

Zhao, H., Liu, C., Wang, F., Wang, J., Li, Q., and Yao, Y., 2007 Uplift time and evolution of Helan Mountain . SCIENTIA SINICA Terrae 37, 185–192 (in Chinese with English abstract).

Zhao, H., Zhang, J., Qu, J., Zhang, B., Yun, L., Li, J., Niu, P., and Nie, F., 2020a. Nature of the Eastern Boundary of the Mesozoic Ordos Basin and the Formation of the Lüliangshan Anticline. The Journal of Geology 128, 157–187. doi: 10.1086/707346 2

Zhao, J., Liu, C., Huang, L., Zhang, D., Wang, D., and Wang, D., 2020b. Paleogeography reconstruction of a multi-stage modified intra-cratonic basin—a case study from the Jurassic Ordos Basin, Western North China Craton. Journal of Asian Earth Sciences 190, 104191. doi: 10.1016/j.jseaes.2019.104191

Zhong, X., Sun, X., Gu, Y., Li, X., Guo, B., and Liu, Y., 2019. Early Cretaceous Palynoflora in Zhangye National Geopark and Its palaeoenvironmental significance. Northwestern Geology 52, 241–249. doi: 10.19751/j.cnki.61-1149/p.2019.04.021

Zhou, Z., and Wang, Y., 2010. Vertebrate diversity of the Jehol Biota as compared with other lagerstätten. Sci. China Earth Sci. 53, 1894–1907. doi: 10.1007/s11430-010-4094-9 12

Zhou, Z., 2014. The Jehol Biota, an Early Cretaceous terrestrial Lagerstätte: New discoveries and implications. National Science Review 1, 543–559. doi: 10.1093/nsr/nwu055 4

Zhou, Z., and Wang, Y., 2017. Vertebrate assemblages of the Jurassic Yanliao Biota and the Early Cretaceous Jehol Biota: Comparisons and implications Palaeoworld 26, 241–252. doi: 10.1016/j.palwor.2017.01.002

Zhu, R., Zhang, H., Zhu, G., Meng, Q., Fan, H., Yang, J., Wu, F., Zhang, Z., and Zheng, T., 2017. Craton destruction and related resources. Int J Earth Sci (Geol Rundsch) 106, 2233–2257. doi: 10.1007/s00531-016-1441-x 7